PERGAMON

International Journal of Solids and Structures 39 (2002) 2927–2937

INTERNATIONAL JOURNAL OF SOLIDS and STRUCTURES

www.elsevier.com/locate/ijsolstr

# Model for measurement of thermal expansion coefficient of concrete by fiber optic sensor

Qingbin Li [a,*], Libo Yuan [b], Farhad Ansari [c]

[a] *Department of Hydraulic Engineering, Tsinghua University, Beijing 100084, PR China*
[b] *Department of Physics, Harbin Engineering University, Harbin 150001, PR China*
[c] *Department of Civil and Materials Engineering, University of Illinois at Chicago, 842 W. Taylor St., Chicago, IL 60607-7023, USA*

Received 11 September 2001; received in revised form 16 February 2002

**Abstract**

The existence of a coating on an optical fiber results in a difference between the strain of the matrix concrete and that sensed by the embedded fiber optic sensor. This paper deals with the theoretical model for measurement of thermal expansion coefficient of concrete by embedded fiber optic sensor. The fiber core, the coating of the optical fiber, and the matrix concrete were all supposed to be elastic. And the bonding surfaces were supposed to be intact, that is to say, there is no relative slip deformation at the interface between the matrix concrete and the coating of the optical fiber, and that between the coating and the fiber core. Based on these assumptions, a theoretical model was developed for measurement of thermal expansion coefficient of concrete. Some experiments were done to verify the validation of the theoretical model. And the comparison indicates a good agreement between the experimental and theoretical results. © 2002 Published by Elsevier Science Ltd.

*Keywords:* Fiber optic sensor; Interface; Measurement; Elasticity; Uniaxial compression; Uniaxial tension; Shear stress; Internal strain; Thermal expansion coefficient; Cement; Concrete

## 1. Introduction

Over the past decade, a variety of fiber optic sensor configurations have been developed for measurement of strains and deformations in structures (Nanni et al., 1991; Ansari, 1993; Eric, 1994; Ansari, 1998; Yuan and Ansari, 1998; Yuan and Zhou, 1998; Li and Ansari, 2001). Fiber optic sensors can be embedded in various kinds of structures such as buildings, roads, dams, and other concrete structures to monitor their strains. Some applications can be found in Li et al. (2002). The optical fiber itself can be divided into two basic types: single mode and multimode fibers. Normally, the former can be used as localized or mechanical sensors, such as strain or force sensors, while the latter can be used as sensors in a more wide range such as

* Corresponding author. Tel.: +86-10-62771015; fax: +86-10-62782159.
*E-mail address:* qingbli@hotmail.com (Q. Li).

0020-7683/02/$ - see front matter © 2002 Published by Elsevier Science Ltd.
PII: S0020-7683(02)00248-2

distributed, environmental, thermal and other sensors. This paper was concentrated on the single mode strain sensor to measure the thermal expansion coefficient of concrete based on interferometer theory.

Thermal expansion is an important factor in all types of structures (Laplante and Boulay, 1994) where differential heating may occur, either from environmental effects, such as the solar heating of pavements and bridge decks, or from service conditions, such as in nuclear-reactor pressure vessels or furnace installations. Failure to allow for thermal expansion, or for thermal stresses resulting from differential expansion, will cause failure. The differential expansion that occurs between cement paste and aggregate will give rise to high internal stresses, which may be critical in the case of large temperature changes.

The thermal expansion coefficient will be a variable quantity depending on the mix design and the type of aggregate used. Since aggregates make up the bulk of concrete, their properties will largely determine the concrete properties. In a mortar, the coefficient of thermal expansion of concrete can be measured though the linear length variation caused by temperature. However, the change in length of a mortar bar is too small to be directly measured with simple instruments.

To deduce the thermal expansion coefficient of a matrix material, the strain of the material with temperature change must be known. In order to know the strain of the matrix material, a relationship between the strain indicated by the fiber optic sensor and that actually applied to the matrix material must be known in advance. For the case depicted in this paper, a single mode optical fiber employed for the interferometer sensor is composed of three circumferential layers. They are: glass core, glass cladding, and protective coating. In fact, the properties of the glass core and glass cladding are almost the same, and they are usually considered as one kind of material and called as fiber core (Ansari and Yuan, 1998). In this paper, a theoretical model for measurement of the thermal expansion coefficient for concrete will be derived.

## 2. Theoretical model

The analysis pertains to the case shown in Fig. 1 (a detailed description will be given in the experimental system section). The optical fiber is embedded in a matrix concrete specimen. A linear segment of the optical fiber and the frame of reference describing the coordinates and dimensional relationships within various layers of the optical fiber are depicted in Fig. 2 with the force distribution. In this figure, $r_a$ and $r_b$ represent the radius of the fiber core and the protective coating, respectively. Shearing stresses at the interface between the core and the protective coating and those between the protective coating and the matrix

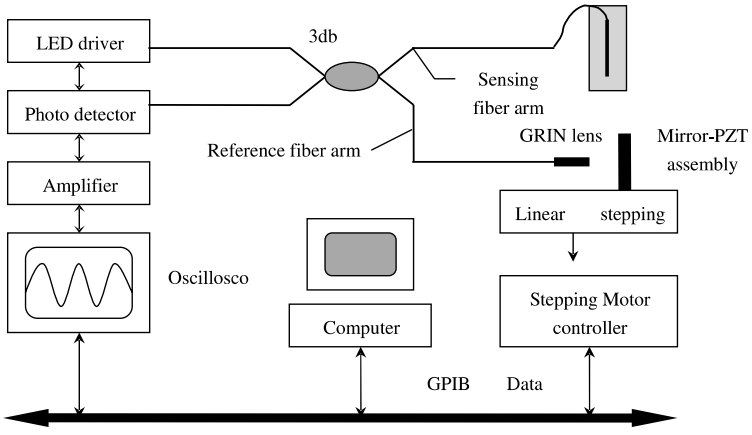


Fig. 1. Overall view of the fiber optic experimental set-up.

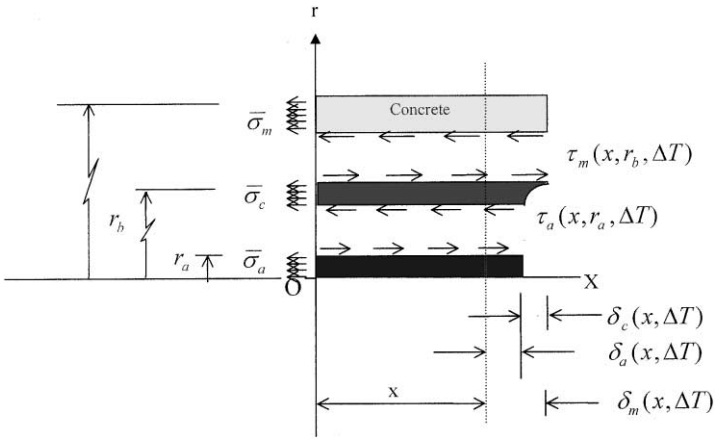


Fig. 2. Sketch of forces of fiber-concrete system.

induced from the discontinuity of deformation between the two different materials are given by $\tau_a(\xi, r_a, \Delta T)$ and $\tau_m(\xi, r_b, \Delta T)$ respectively. Here $\Delta T$ is the temperature change. The basic assumptions and requirements pertinent to the development of the model are given below:

(1) The theory is applicable as long as all of the materials involved including the optical fiber core, protective coating and the matrix concrete behave in a linear elastic manner.
(2) Perfect bond exists at the matrix/coating, and at the coating/core interfaces. This assumption is grossly true. It ignores the local imperfections along the interface in the formulation of the governing equations.
(3) Mechanical properties of the core and cladding are considered the same. For simplicity, they are collectively referred to as the fiber core.
(4) The model does not take into account the effect of radial stress. No mechanical stress is loading on the structure.

For the fiber segment shown in Fig. 2, the analysis begins by imposing force equilibrium at arbitrary section through the coating, i.e. $r_a < r < r_b$,

$$\pi(r^2 - r_a^2)\bar{\sigma}_c + 2\pi r_a \int_0^L \tau_a(r_a, \xi, \Delta T)\,d\xi - 2\pi r \int_0^L \tau(r, \xi, \Delta T)\,d\xi = 0 \tag{1}$$

where $\bar{\sigma}_c$ is uniform normal stress at the central cross section of the coating, $\tau(r, \xi, \Delta T)$ is the distribution of the shear stress at arbitrary section through the coating, i.e. $r_a < r < r_b$, Eq. (1) can also be rewritten as

$$\frac{1}{L}\int_0^L (r^2 - r_a^2)\bar{\sigma}_c\,d\xi + 2r_a \int_0^L \tau_a(r_a, \xi, \Delta T)\,d\xi - 2r \int_0^L \tau(r, \xi, \Delta T)\,d\xi = 0 \tag{2}$$

Since $\tau(r, \xi)$ and $\tau_g(r_g, \xi)$ are uniform, the following equation can be obtained from Eq. (2):

$$\frac{1}{L}(r^2 - r_a^2)\bar{\sigma}_c + 2r_a\tau_a(r_a, \xi, \Delta T) - 2r\tau(r, \xi, \Delta T) = 0 \tag{3}$$

Since $L \gg r^2$, the first term of left hand side in Eq. (3) approaches to zero. Then we get the distribution of the shear stress, $\tau(r, x)$, at arbitrary section through the coating, i.e. $r_a < r < r_b$, as:

$$\tau(r,x)=\frac{r_{\mathrm{g}}}{r}\tau_{\mathrm{g}}(r_{\mathrm{g}},x) \tag{4}$$

The condition of compatibility governing the axial deformation of the optical fiber is employed for the determination of $\tau_{\mathrm{a}}(x,r_{\mathrm{a}},\Delta T)$ as follows:

$$\delta_{\mathrm{m}}(x,\Delta T)=\delta_{\mathrm{a}}(x,\Delta T)+\delta_{\mathrm{c}}(x,\Delta T) \tag{5}$$

where $\delta_{\mathrm{m}}(x,\Delta T)$ is the deformation of the matrix concrete, $\delta_{\mathrm{a}}(x,\Delta T)=\delta(x,r_{\mathrm{a}},\Delta T)$ is the total deformation of the optical fiber core caused by the glass fiber thermal expansion and the normal stress inside the glass fiber, and $\delta_{\mathrm{c}}(x,\Delta T)=\delta(x,r_{\mathrm{c}},\Delta T)$ is the shear deformation of the protective coating at the coating/matrix interface, depending on the interfacial shear stresses between matrix-coating and coating-glass fiber core. The deformation terms in Eq. (5) can be determined by using the Hooke's law. To determine $\delta_{\mathrm{c}}(x,\Delta T)$, we have:

$$\tau(x,r,\Delta T)=G_{\mathrm{c}}\gamma_{\mathrm{c}}(x,r,\Delta T) \tag{6}$$

where $\gamma_{\mathrm{c}}(x,r,\Delta T)$ is the shear strain, $G_{\mathrm{c}}=E_{\mathrm{c}}/2(1+v_{\mathrm{c}})$ is the shear modulus of the protective coating. $E_{\mathrm{c}}$ and $v_{\mathrm{c}}$ represent the Young's modulus and Poisson's ratio of the protective coating respectively. For the case of small deformation, $\gamma_{\mathrm{c}}(x,r,\Delta T)=\mathrm{d}x/\mathrm{d}r$ is true. Thus, $\delta_{\mathrm{c}}(x,\Delta T)$ can be expressed in the following manner:

$$\delta_{\mathrm{c}}(x,\Delta T)=\int_{x}^{x+\delta_{\mathrm{c}}}\mathrm{d}x=\int_{r_{\mathrm{a}}}^{r_{\mathrm{b}}}\frac{\tau r_{\mathrm{a}}(x,r_{\mathrm{a}},\Delta T)}{G_{\mathrm{c}}(T)}\frac{r_{\mathrm{a}}}{r}\,\mathrm{d}r=\frac{r_{\mathrm{a}}}{G_{\mathrm{c}}(T)}\tau_{\mathrm{a}}(x,r_{\mathrm{a}},\Delta T)\ln\left(\frac{r_{\mathrm{b}}}{r_{\mathrm{a}}}\right) \tag{7}$$

The longitudinal deformation of the matrix material and the core of the optical fiber are given by:

$$\delta_{\mathrm{m}}(x,\Delta T)=\alpha_{\mathrm{m}}x(\Delta T)-\int_{0}^{x}\frac{\sigma_{\mathrm{m}}(\xi,\Delta T)}{E_{\mathrm{m}}}\,\mathrm{d}\xi \tag{8}$$

$$\delta_{\mathrm{a}}(x,\Delta T)=\alpha_{\mathrm{f}}x(\Delta T)+\int_{0}^{x}\frac{\sigma_{\mathrm{f}}(\xi,\Delta T)}{E_{\mathrm{f}}}\,\mathrm{d}\xi \tag{9}$$

In which $\sigma_{\mathrm{m}}(x,\Delta T)$ and $E_{\mathrm{m}}$ represent the normal stress and modulus of elasticity of the matrix material respectively, $\sigma_{\mathrm{a}}(x,\Delta T)$ and $E_{\mathrm{f}}$ are normal stress and modulus of elasticity pertaining to the fiber core respectively, $\alpha_{\mathrm{m}}$ and $\alpha_{\mathrm{f}}$ are thermal expansion coefficients of the matrix concrete and the fiber core respectively. Imposing force equilibrium at arbitrary section through the fiber core, $\sigma_{\mathrm{a}}(x,\Delta T)$ is derived as:

$$\sigma_{\mathrm{a}}(x,\Delta T)=\bar{\sigma}_{\mathrm{a}}-\frac{2}{r_{\mathrm{a}}}\int_{0}^{x}\tau_{\mathrm{a}}(\xi,r_{\mathrm{a}},\Delta T)\,\mathrm{d}\xi \tag{10}$$

where $\bar{\sigma}_{\mathrm{a}}$ is the uniform normal stress at the central cross section of the fiber core. In the same way as used before, the normal stress at the arbitrary cross section inside the matrix concrete can be, accounting for Eq. (4), obtained as

$$\sigma_{\mathrm{m}}(x,\Delta T)=\frac{2\pi r_{\mathrm{a}}}{A_{\mathrm{m}}}\int_{x}^{L}\tau_{\mathrm{a}}(\xi,r_{\mathrm{a}},\Delta T)\,\mathrm{d}\xi \tag{11}$$

in which, $A_{\mathrm{m}}$ is the area of the cross section of matrix material.Substitutions of Eq. (11) in Eq. (8) and Eq. (10) into Eq. (9) yield the following forms:

$$\delta_{\mathrm{m}}(x,\Delta T)=\alpha_{\mathrm{m}}x(\Delta T)-\frac{2\pi r_{\mathrm{a}}}{A_{\mathrm{m}}E_{\mathrm{m}}}\int_{0}^{x}\left(\int_{x}^{L}\tau_{\mathrm{a}}(\xi,r_{\mathrm{a}},\Delta T)\,\mathrm{d}\xi\right)\mathrm{d}x \tag{12}$$

$$\delta_a(x,\Delta T)=\alpha_f x(\Delta T)+\frac{1}{E_f}\int_0^x\left(\bar{\sigma}_a-\frac{2}{r_a}\int_0^x\tau_a(\xi,r_a,\Delta T)\,d\xi\right)dx \tag{13}$$

Substitution of the right-hand side of Eqs. (7), (12) and (13) into the compatibility condition, Eq. (5), yields

$$\alpha_m(\Delta T)x-\frac{2\pi r_a}{A_mE_m}\int_0^x\left(\int_x^L\tau_a(\xi,r_a,\Delta T)\,d\xi\right)dx=\frac{r_a\ln(r_b/r_a)}{G_c}\tau_a(x,r_a,\Delta T)+\alpha_f x(\Delta T)+\frac{1}{E_f}\int_0^x\left(\bar{\sigma}_a-\frac{2}{r_a}\int_0^x\tau_a(\xi,r_a,\Delta T)\,d\xi\right)dx \tag{14}$$

Differentiation of Eq. (14) yields:

$$\alpha_m(\Delta T)-\frac{2\pi r_a}{A_mE_m}\int_x^L\tau_a(x,r_a,\Delta T)\,dx=\frac{r_a}{G_c(T)}\ln\left(\frac{r_b}{r_a}\right)\tau_a'(x,r_a,\Delta T)+\alpha_f(\Delta T)-\frac{2}{r_aE_f}\int_0^x\tau_a(x,r_a,\Delta T)\,dx \tag{15}$$

Differentiation of Eq. (15) yields:

$$\tau_a''(x,r_a,\Delta T)-k^2\tau_a(x,r_a,\Delta T)=0 \tag{16}$$

where

$$k^2=\frac{\frac{2}{r_aE_f}+\frac{2\pi r_a}{A_mE_m}}{\frac{r_a}{G_c}\ln(r_b/r_a)} \tag{17}$$

Solution to Eq. (16) is of the following form:

$$\tau_a(x,r_a,T)=C_1(\Delta T)\cosh(kx)+C_2(\Delta T)\sinh(kx) \tag{18}$$

where the constants of integration, $C_1(\Delta T)$ and $C_2(\Delta T)$, are determined from the force boundary conditions:

$$\sigma_a(0)=\bar{\sigma}_a \tag{19}$$

$$\sigma_a(L)=0 \tag{20}$$

Hence, by imposing these boundary conditions on Eq. (10), $C_1(\Delta T)$ and $C_2(\Delta T)$ can be evaluated as:

$$C_1(\Delta T)=0,\quad C_2(\Delta T)=\frac{r_ak\bar{\sigma}_a}{2[\cosh(kL)-1]} \tag{21}$$

Substitution of $C_1(\Delta T)$ and $C_2(\Delta T)$ into Eq. (18) yields the function describing the distribution of interfacial shear stresses between the core and the protective coating:

$$\tau_a(x,r_a,\Delta T)=\frac{r_ak\bar{\sigma}_a}{2[\cosh(kL)-1]}\sinh(kx) \tag{22}$$

where $\bar{\sigma}_a$ is unknown till now, but can be determined by substituting Eq. (22) into Eq. (13) as follows:

$$\bar{\sigma}_a=E_f\frac{\frac{\delta_a(L,\Delta T)}{L}-\alpha_f(\Delta T)}{1-\frac{\sinh(kL)-kL}{kL[\cosh(kL)-1]}} \tag{23}$$

It should be noted that $\delta_a(L,\Delta T)$ in Eq. (23) is measured by the fiber optic sensor in the temperature change, $\Delta T$. Theoretically, the shear stress distribution is shown in Fig. 3 with the different temperature

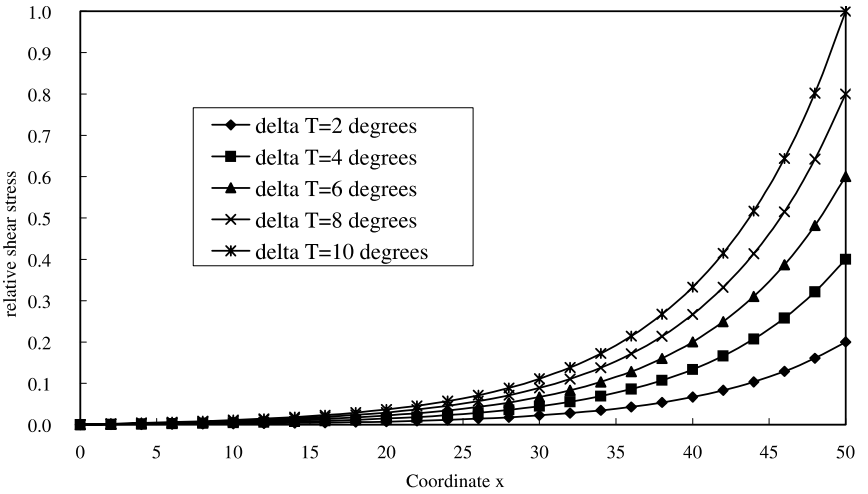


Fig. 3. Distribution of the shear stress at the interface between the fiber core and the protective coating along fiber optic sensor.

changes, $\Delta T = (T - T_0)$. Longitudinal stress distribution in the optical fiber core is determined from subsequent substitution of Eq. (22) into Eq. (10):

$$\sigma_a(x, \Delta T) = \bar{\sigma}_a \frac{\cosh(kL) - \cosh(kx)}{\cosh(kL) - 1} \tag{24}$$

In order to induce the coefficient of expansion of the matrix material, we substitute Eq. (22) into Eqs. (7), (12) and (13), these yield:

$$\delta_c(L, \Delta T) = \frac{k r_a^2 \bar{\sigma}_a \ln\left(\frac{r_c}{r_a}\right) \sinh(kL)}{2G_c[\cosh(kL) - 1]} \tag{25a}$$

$$\delta_a(L, \Delta T) = \alpha_f L(\Delta T) + \frac{\bar{\sigma}_a}{E_f}\left[L - \frac{\sinh(kL) - kL}{2[\cosh(kL) - 1]}\right] \tag{25b}$$

$$\delta_m(L, \Delta T) = \alpha_m L(\Delta T) - \frac{\pi r_a^2 \bar{\sigma}_a}{A_m E_m}\left[\frac{kL\cosh(kL) - \sinh(kL)}{k[\cosh(kL) - 1]}\right] \tag{25c}$$

Substitution of Eqs. (25a), (25b), (25c) into Eq. (5) yields

$$\alpha_m = \alpha_f + \frac{\bar{\sigma}_a}{L(\Delta T)}\left\{\frac{k r_a^2 \ln(r_c/r_a)\sinh(kL)}{2G_c[\cosh(kl) - 1]} + \frac{1}{E_f}\left[L - \frac{\sinh(kL) - kL}{2[\cosh(kl) - 1]}\right] + \frac{\pi r_a^2}{A_m E_m}\left[\frac{kL\cosh(kL) - \sin k(kL)}{k[\cosh(kL) - 1]}\right]\right\} \tag{26}$$

By Eq. (26), one can get the coefficient of thermal expansion of the matrix material. It should be noted that when the matrix is large enough to neglect its deformation induced from normal stress inside, Eq. (26) becomes

$$\alpha_m = \alpha_f + \frac{\bar{\sigma}_a}{L(\Delta T)}\left\{\frac{k r_a^2 \ln(r_c/r_a)\sinh(kL)}{2G_c[\cosh(kL) - 1]} + \frac{1}{E_f}\left[L - \frac{\sinh(kL) - kL}{2[\cosh(kL) - 1]}\right]\right\} \tag{27}$$

## 3. Experimental system

Michelson interferometers have been extensively employed for characterization of laser and light emitting diodes (LED) in terms of coherence length. Coherence length of a light source pertains to the ability of the lightwave to retain a stable phase difference in time. Lasers are capable of producing single wavelength emissions possessing long coherent lengths. On the other hand LED's produce white light of low coherence. A white light supplier such as an LED produces broad band emissions, or emissions containing a wide range of wavelengths (wide spectrum). In a Michelson white light interferometer arrangement, light from an LED is split into two beams, as shown in Fig. 4. One of the beams travels a fixed distance (reference beam). The path length of the other beam is variable. Then the beams are recombined. If the path length of the variable beam of light made equal to that of the reference beam, then an interference pattern similar to that given in Fig. 5 is generated. The difference in path length over which the interference pattern resides is used for the determination of coherence length. This same technique can be utilized as a powerful tool for measurement of deformations and strains. A fiber optic sensor based on the Michelson white light interferometer is depicted in Fig. 1. The measurement system is comprised of an LED, a fiber optic coupler for separating and recombining the light, two optical fiber arms with partially reflective surfaces, and a scanning mirror mounted on a stepper motor positioning system. The length of the fiber

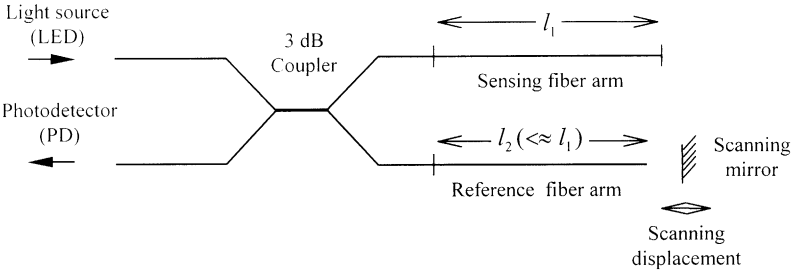


Fig. 4. Fiber optic white light interferometer strain sensor system.

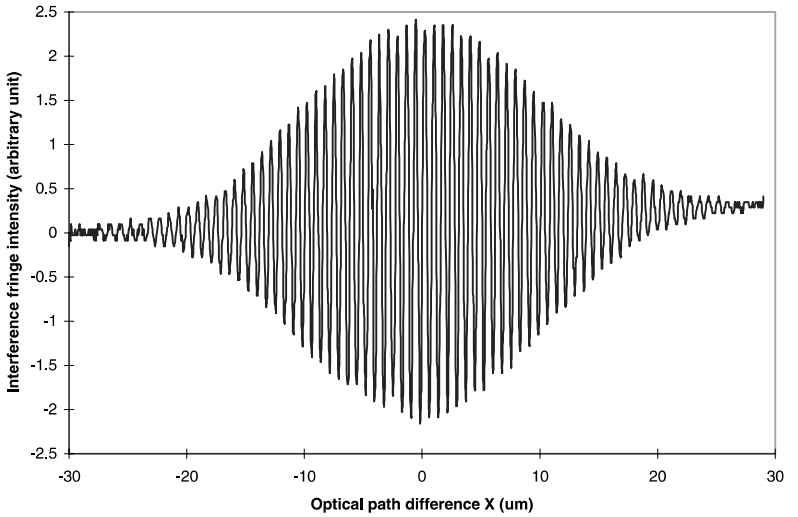


Fig. 5. Output of fiber optic white light interferometer illuminated by a LED source with central wavelength 1300 nm.

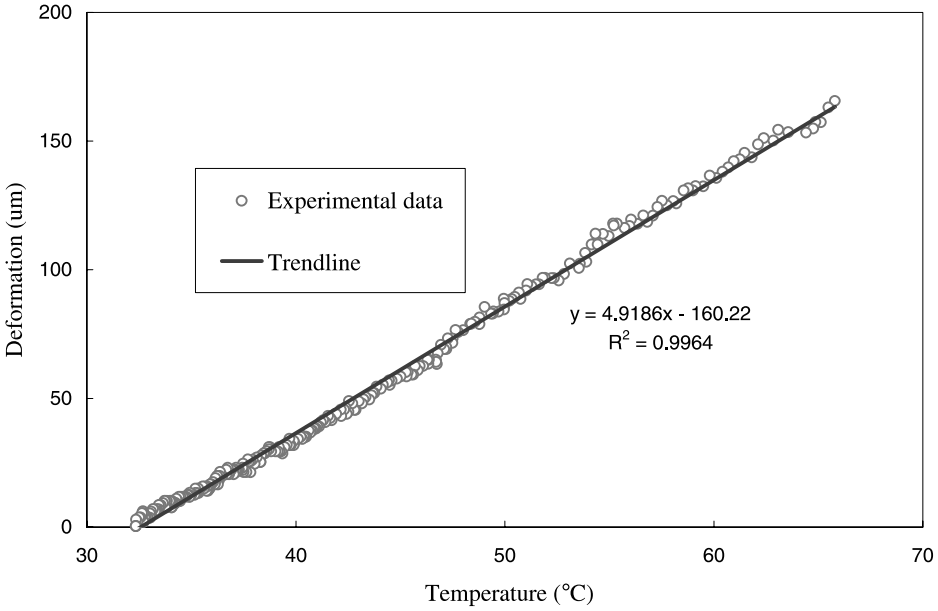


Fig. 6. Deformation of fiber embedded in cement vs. temperature.

optic sensor arm is fixed, and the reference arm is made slightly shorter than the sensing arm (about 1–2 mm). Separate beams of light travel through the reference and the sensing arms of the optical fiber. The reflective surfaces define the gauge length of the sensor. The reflective surfaces in both of the optical fibers guide the light back to a detector by way of a coupler. The sensing arm is embedded in the mortar bar under test. In the start position, the mirror scans a short distance in front of the reference arm. Once the sum of the scanned distance plus the length of the reference arm equal that of the sensing arm white light fringes similar to that given in Fig. 5 appear. The zero order fringe which is approximately in the center of fringe pattern and has the highest amplitude corresponding to the exact optical path matching of these two beams. This procedure can be repeated for locating the new white light fringe pattern due to thermal expansion of the sensing arm. As shown in Fig. 6, the distance between the zero-order fringe patterns for the undeformed and deformed positions gives the amount of the optical path that changes in gauge length $2L$. The interferometric fiber optic sensor provides for a high-resolution absolute deformation measurement capability. The sensitivity of the measurements depends on the resolution of the scanning mirror. For this reason, in the present study experiments, a high-resolution stepper motor (1 μm step intervals) was employed for coarse scanning of the distance, and the piezoelectric actuator (sub-micron resolution) was used for a fine tuning of the location of the fringe pattern. The procedure can be repeated for measurement of successive deformations by way of automation.

The displacement of the mirror is equal to the optical path changing of the fiber with the gauge length $2L$ it can be expressed as

$$\Delta x = 2[n\Delta L(\varepsilon_f) + \Delta n(\varepsilon_f)L] \tag{28}$$

where $\Delta x$ is the displacement of the scanning mirror. The first term $\Delta L(\varepsilon_f)$ at the right side in Eq. (28) represents the physical change of optical fiber length produced by the strain, it is directly related to axial strain $\varepsilon_f(x, \Delta T)$ induced by thermal expansion through the expression

$$\Delta L(\varepsilon_f) = L\varepsilon_f \tag{29}$$

The second term, the change in optical path due to a change in the refractive index of the fiber core, it is given by

$$\Delta n = -\frac{1}{2}n^3[(1-\mu)p_{12} - \mu p_{11}]\varepsilon_f \tag{30}$$

Thus, we have

$$\begin{aligned}\Delta x &= 2\left\{nL\varepsilon_f - \frac{1}{2}n^3[(1-\mu)p_{12} - \mu p_{11}]L\varepsilon_f\right\} \\ &= 2\left\{n - \frac{1}{2}n^3[(1-\mu)p_{12} - \mu p_{11}]\right\}L\varepsilon_f \\ &= 2n_{\text{eff}}L\varepsilon_f(x,\Delta T)\end{aligned} \tag{31}$$

where $n_{\text{eff}} = n - \frac{1}{2}n^3[(1-\mu)p_{12} - \mu p_{11}]$ represents the effective refractive index of the fiber core. For the silica materials at wavelength $\lambda = 1300$ nm, the parameters are $n = 1.46$, Poisson ratio $\mu = 0.25$, and photoelastic constants $p_{11} \approx 0.12$, and $p_{12} \approx 0.27$ are taken from Ansari and Yuan (1998). Using these data, the effective index can be calculated as $n_{\text{eff}} \approx 1.19$.

## 4. Results

In order to measure the thermal expansion coefficient of concrete materials, a 305 mm length single-mode optical fiber is embedded in the same length mortar bar. The cross section of which is $25 \times 25$ mm$^2$. The specimen was cured in a standard curing room for 7 days, and then moved out to the air in a normal room. Before the test, the specimen was saturated in water with room temperature for 24 h. Put the mortar bar into the temperature chamber along with the same length reference fiber in order to eliminate the influence due to the part of optical fiber outside the mortar.

The result for the pure cement paste mortar bar with the cement water ratio = 1:0.46 is shown in Fig. 6, and its thermal expansion coefficient can be calculated as $\alpha_{CW} = 17.5 \times 10^{-6}$/°C by Eq. (27) and the data given by Table 1. It is very close to the normal values of cement, $11–20 \times 10^{-6}$/°C (Neville, 1981).

Fig. 7 corresponds to the testing results measured by the mortar bar mixed by cement and sand with the ratio = 1:0.46:2.43 corresponding to cement, water and sand. The thermal expansion coefficient for this kind material can be calculated as $\alpha_{CSW} = 15.8 \times 10^{-6}$/°C. It is consistent with the normal domain of these values, $10.1–18.5 \times 10^{-6}$/°C (Neville, 1981).

Table 1
The data of materials characteristics

| Materials parameters | Symbols | Values | Unit |
|---|---|---|---|
| Young's modulus of the glass material | $E_f$ | $7.2 \times 10^{10}$ | Pa |
| Young's modulus of the cement paste material | $E_m$ | $1.8 \times 10^{10}$ | Pa |
| Young's modulus of the cement and sands paste material | $E_m$ | $2.0 \times 10^{10}$ | Pa |
| Young's modulus of the concrete material | $E_m$ | $2.4 \times 10^{10}$ | Pa |
| Poisson's ratio of silicon coating material | $v_c$ | 0.499 | – |
| Shear modulus of the protective coating material | $G_c$ | $8.5 \times 10^5$ | Pa |
| Optical fiber length embedded in matrix | $2L$ | 305 | mm |
| Radius of the outer boundary of the protective | $r_b$ | 102.5 | μm |
| Glass fiber radius | $r_a$ | 62.5 | μm |
| Thermal coefficient of glass fiber | $\alpha_f$ | $5.5 \times 10^{-7}$ | 1/°C |
| Parameter $k$ | $k$ | 0.11 | 1/mm |

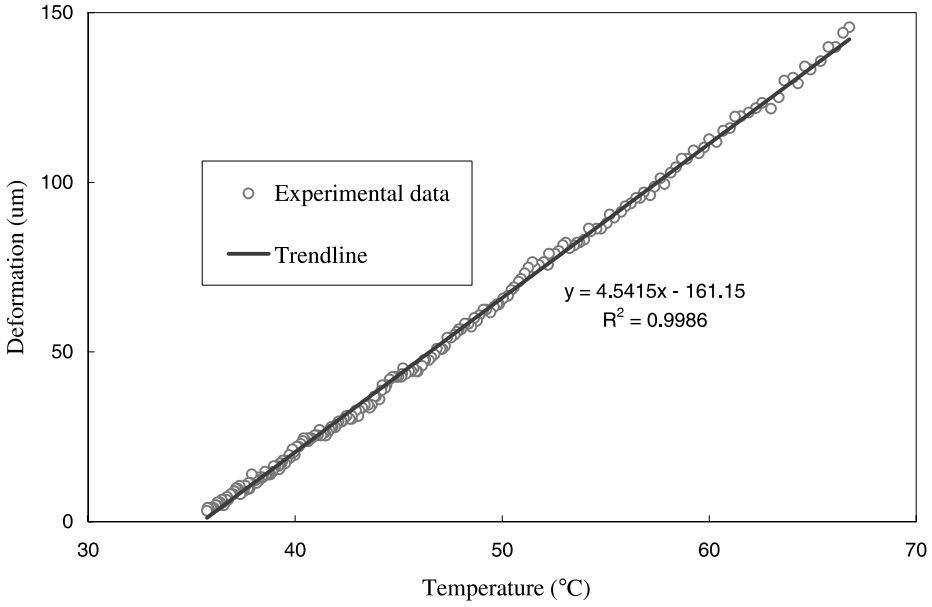


Fig. 7. Deformation of fiber embedded in cement vs. temperature.

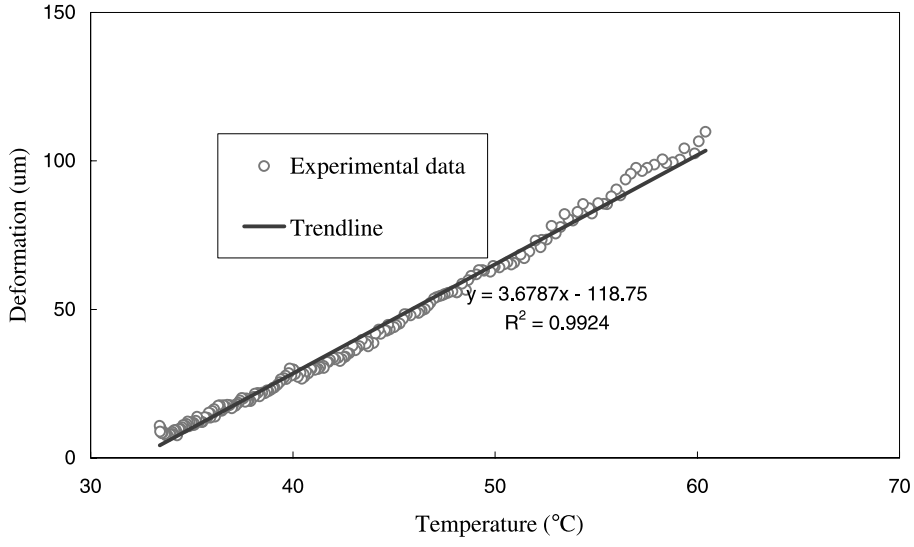


Fig. 8. Deformation of fiber embedded in mortar bar vs. temperature.

For concrete material, the experimental results are illustrated in Fig. 8. The mix proportion by weight of the concrete used in this mortar bar were 1:2.43:2.74:0.46 corresponding to cement:sand:aggregate:water. The thermal expansion coefficient for this kind of concrete is $\alpha_{CSAW} = 12.8 \times 10^{-6}/°C$. It is also consistent with the normal domain of these values, 7.4–13.1 $\times 10^{-6}/°C$ (Neville, 1981).

## 5. Conclusions

In this paper, the theoretical model for measurement of thermal expansion coefficient of concrete by embedded fiber optic sensor was proposed. The fiber core, the coating of the optical fiber, and the matrix concrete were supposed to be elastic materials. All the bonding surfaces were supposed to be intact, that is to say, there is no relative slip deformation at the interfaces. Some experiments were done to verify the validation of the theoretical model. The previous study supports the following conclusions:

1. Based on the elasticity theory, the shear transferring of the fiber optic sensor can be determined. And the strain-transferring coefficient can also be determined for the fiber optic sensor embedded in concrete mortar bar with temperature change.
2. The theoretical model for measurement of thermal expansion coefficient of concrete can be used for practical application, which possess a similar precision to the normal method.

## Acknowledgements

This work was partly supported by the grants from The Chinese Ministry of Education for back overseas students, from Natural Science Foundation of China, and from 985 project of Tsinghua University.

## References

Ansari, F. (Ed.), 1993. Application of Fiber Optic Sensors in Engineering Mechanics. ASCE, New York, NY.

Ansari, F., 1998. Fiber Optic Sensors for Construction Materials and Bridges. Technomic Publishing Company Inc., Lancaster, PA.

Ansari, F., Yuan, L., 1998. Mechanics of bond and interface shear transfer in optical fiber sensors. J. Engrg. Mech.-ASCE 124 (4), 385–394.

Eric, U., 1994. Fiber Optic Smart Structure. John Wiley & Sons Inc., New York, USA.

Laplante, P., Boulay, C., 1994. Evolution of the thermal-expansion coefficient of concrete as a function of its maturity at very early ages. Mater. Struct. 27 (174), 596–605.

Li, Q., Ansari, F., 2001. Circumferential strain measurement of high strength concrete in triaxial compression by fiber optic sensor. Int. J. Solids Struct. 38 (42-43), 7607–7625.

Li, Q., Li, G., Wang, G., Ansari, F., Liu, Q., 2002. Elasto-Plastic Bonding of Embedded Optical Fiber Sensors in Concrete. J. Engrg. Mech.-ASCE 128 (4), 471–478.

Nanni, A., Yang, C.C., Pan, K., Wang, J.-S., Michael, R.R., 1991. Fiber-optic sensors for concrete strain/stress measurement. J. ACI Mater. J. 88 (4), 257–264.

Neville, A.M., 1981. Properties of Concrete, third ed. Pitman Publishing Limited, London.

Yuan, L., Zhou, L., 1998. Sensitivity coefficient evaluation of embedded fiber-optic strain sensor. J. Sensors Actuators A 69 (1), 5–11.

Yuan, L., Ansari, F., 1998. Embedded white light interferometer fiber optic strain sensor for monitoring crack-tip opening in concrete beams. J. Meas. Sci. Technol. 9 (2), 261–266.